Unified minimum effective model of magnetic properties of iron-based superconductors

Jiangping Hu,[1,2,*] Bao Xu,[1] Wuming Liu,[1] Ning-Ning Hao,[1] and Yupeng Wang[1]

[1]*Beijing National Laboratory for Condensed Matter Physics and Institute of Physics, Chinese Academy of Sciences, P.O. Box 603, Beijing 100190, China*

[2]*Department of Physics, Purdue University, West Lafayette, Indiana 47907, USA*

(Received 1 October 2011; revised manuscript received 14 March 2012; published 3 April 2012)

Iron-based superconductors exhibit many different antiferromagnetically ordered ground states. We construct a minimum effective magnetic model that displays all magnetic phases. This model also captures three incommensurate magnetic phases as well, two of which have been observed experimentally. The model characterizes the nature of phase transitions between the different magnetic phases and explains a variety of magnetic properties, such as spin-wave spectra and electronic nematism. Most importantly, by unifying the understanding of magnetism, we cast insight on the key ingredients of magnetic interactions that are critical to the occurrence of superconductivity.

DOI: 10.1103/PhysRevB.85.144403 PACS number(s): 74.25.Ha, 74.20.De, 74.70.Xa, 75.50.Ee

I. INTRODUCTION

Since 2008, many families of iron-based high-temperature (high-T_c) superconductors have been discovered.[1–4] Unlike all parent compounds of cuprates that share a common antiferromagnetically (AF) ordered ground state, those of iron-based superconductors exhibit many different AF ordered ground states, including collinear-AF (CAF) state in ferropnictides[5] as shown in Fig. 1(a), bicollinear-AF (BCAF) state in 11-ferrochalcogenide FeTe[6,7] as shown in Fig. 1(b), and block-AF vacancy (BAF_v) order state in 122-ferrochalcogenide $K_{0.8}Fe_{1.6}Se_2$[8] as shown in Fig. 1(d). While the universal presence of antiferromagnetism suggests that superconductivity is strongly interrelated with magnetism, the diversity of the AF ordered states obscures their interplay.

Theoretically, because of the diversity of the magnetic orders and the fact that the magnetic properties exhibit the dichotomic behavior of both local moment and itinerant electron aspects, it has been extremely difficult to find a consistent magnetic model to describe the magnetism of iron-based superconductors. Magnetism can be explained by either local moment models where local spins interact with each other or itinerant electron models where magnetic order arises from nested Fermi surfaces. The former is appropriate for insulating materials such as the parent compounds of cuprates, while the latter is suitable for metallic systems, such as chromium. However, the iron-based superconductors include rather diversified materials whose parent compounds can have either metallic or insulating ground states. More specifically, the parent compounds of ferropnictides are bad metals,[1] while the discovered 122-ferrochalcogenide, $K_{0.8}Fe_{1.6}Se_2$ is a block AF insulator.[8,9] Moreover, it was shown that even in the insulating parent compounds, itinerant electron aspects have to be included[10] and in the metallic parent compounds, local moment aspects are manifested.[11] Such a dichotomy of the magnetic properties[10–16] leads to many diversified viewpoints on what is the proper model to describe the magnetism[10,17–28].

Here, we attempt to formulate a minimum effective spin model that unites the description of the magnetic properties of the parent compounds of the different classes of iron-based superconductors. The model has to preserve the tetragonal lattice symmetry so that it is capable of providing us the detailed relations between different magnetically ordered states as consequences of spontaneous symmetry breaking at low temperature. The model should be able to capture all the magnetically ordered ground states observed in iron-based superconductors, to explain their correct spin-wave spectra and the anisotropy of magnetic exchange interactions, and to predict possible states including incommensurate magnetic states. In the following, we will show by including the nearest-neighbor (NN) biquadratic interaction term as proposed in Ref. 20, but not the next-nearest-neighbor (NNN) biquadratic interaction term, and the next-next-nearest-neighbor (NNNN) AF Heisenberg interactions J_3[29,30] in $J_1 - J_2 - J_c$ model,[18] we can fulfill above requirements.

II. MODEL AND PHASE DIAGRAM

We start with the following general Hamiltonian:

$$H = \sum_{ij,n} \left[J_{ij} \vec{S}_i^n \cdot \vec{S}_j^n - K_{ij} \left(\vec{S}_i^n \cdot \vec{S}_j^{,n} \right)^2 \right] + J_c \sum_{i,n} \vec{S}_i^n \cdot \vec{S}_i^{n+1}, \tag{1}$$

where n labels layer, J_{ij} describes inplane magnetic exchange interactions, J_c is interplane magnetic coupling along c axis (between iron layers), and K_{ij} are inplane non-Heisenberg biquadratic couplings. In the minimum model proposed here, we choose nonvanishing $J_{ij} = J_1$, J_2, or J_3 if and only if i, j are two NN, NNN, or NNNN sites, respectively, and $K_{ij} = K$ if and only if i, j are two NN sites. The interactions are sketched in Fig. 1(a) by the dashed lines. We note that the model is a natural unification of models in Refs. 18,20,29 and 30 proposed for ferropnictides and ferrochalcogenides before. However, all previous models only describe particular family and fail to provide a comprehensive understanding of different magnetic states.

The classical phase diagram of the model can be obtained exactly (see Appendix A). In Fig. 2, we draw a typical phase diagram in the $J_3/|J_1|$-$J_2/|J_1|$ plane by taking $KS^2/|J_1| = 0.2$. The phase diagram is almost symmetric between $J_1 > 0$ (the right part of Fig. 2) and $J_1 < 0$ (the left part of Fig. 2). For $J_1 > 0$, there are three regions for commensurate phases labeled as AFM, CAF, BCAF in Fig. 2, which exactly describe

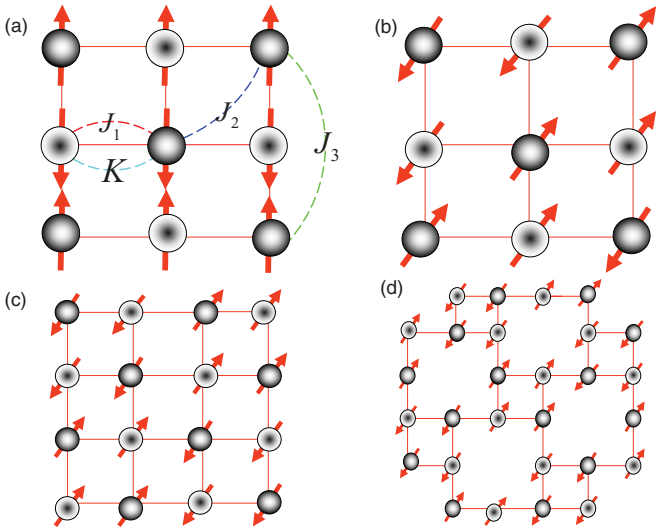

FIG. 1. (Color online) (a) The collinear-antiferromagnetic state (CAF) in ironpnictides, for example, $CaFe_2As_2$. (b) The bicollinear-antiferromagnetic state (BCAF) in FeTe. (c) the block-antiferromagnetic state (BAF) without iron vacancies. (d) The block-antiferromagnetic state with $\sqrt{5}\times\sqrt{5}$ vacancy ordering (BAF_v) in $K_{0.8}Fe_{1.6}Se_2$. The exchange couplings are indicated in (a).

the static magnetic states of the parent compounds of curpates, ferropnictides, and 11-ferrochalcogenide FeTe, respectively. Intriguingly, a block-AF (BAF) commensurate state as shown in Fig. 1(c) is degenerate with the BCAF state. The difference between them is that the BCAF state breaks the C^4 rotation symmetry of the tetragonal lattice while the BAF does not. The spin configuration of the BAF state is the same as the BAF_v state except that there is no vacancy. Therefore the model really captures all commensurate magnetic states in iron-based superconductors and also suggests a BAF state. There are also two incommensurate phases sandwiched between the commensurate phases with ordered incommensurate wave vectors (q,π) or (π,q) (labeled as IC1) and (q,q) (labeled as IC3), respectively. The static (q,q) phase was observed in

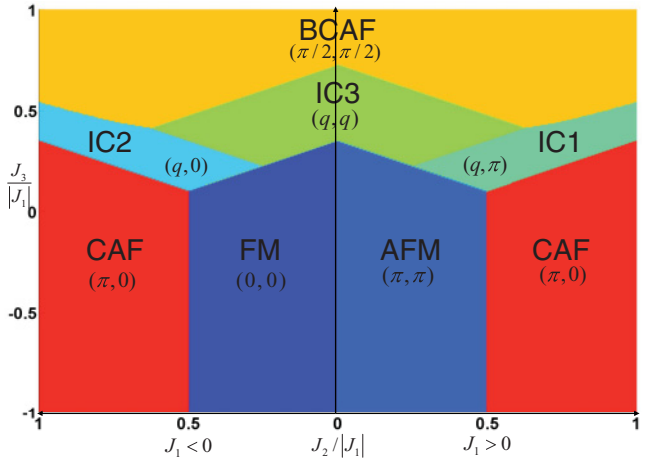

FIG. 2. (Color online) The classical phase diagram of the $J_1-J_2-J_3-K$ model at $K=0.2J_1$. There are total four commensurate and three incommensurate magnetic phases. Their labels and the ordered wave vectors are specified in the figure.

$Fe_{1+y}Te$ when $y>0.1$.[6] Although no static (q,π) phase has been detected, the (q,π) incommensurate spin fluctuations have been observed in $FeTe_{1-x}Se_x$,[31,32] electron-overdoped $Ba(Fe_{1-x}Co_x)_2As_2$,[33] and hole-doped KFe_2As_2.[34] If J_1 is switched to negative, namely ferromagnetic (FM), the AFM phase becomes a FM phase and (q,π) becomes $(q,0)$ or $(0,q)$ (labeled as IC2).

More specifically, we can determine phase transition boundary. We scale other parameters with J_1 as $\tilde{K}=KS^2/J_1$, $\tilde{J}_2=J_2/J_1$, and $\tilde{J}_3=J_3/J_1$ for simplicity. The phase boundary between the BCAF and the (q,π) incommensurate phase is determined by $4(\tilde{J}_3-\frac{1}{4})^2-(\tilde{J}_2-\frac{1}{2})^2=(\tilde{K}-\frac{1}{2})^2$ that defines the upper branch of a hyperbolic curve centered at $(\tilde{J}_2,\tilde{J}_3)=(1/2,1/4)$. The phase boundary between the AFM and BCAF phases is determined by $\tilde{J}_3=-\frac{1}{2}\tilde{J}_2+\frac{1}{2}$ and that between BCAFM and CAFM phases is determined by $\tilde{J}_3=\frac{1}{2}\tilde{J}_2$. The incommensurate states appear only when $\tilde{K}<0.5$. We emphasize that finite positive $\tilde{K}>(1.5-\sqrt{2})$ and $\tilde{J}_3>0.25$ are necessary conditions for the appearance of the BCAF phase. The incommensurate wave vectors of the three incommensurate phases can also be explicitly determined: (1) $(q,0)$ or $(0,q)$ phase with $q=\arccos\frac{2\tilde{J}_2+1}{2\lambda}$, (2) (q,π) or (π,q) with $q=\arccos\frac{1-2\tilde{J}_2}{2\lambda}$, and (3) (q,q) with $q=\arccos\frac{1}{2(\tilde{J}_2-\lambda)}$, where $\lambda=\tilde{K}-2\tilde{J}_3$.

III. SPIN EXCITATIONS AND EFFECTIVE EXCHANGE COUPLINGS

Now we discuss each phase and their associated experimental observations. First, the model captures four commensurate phases: AFM, CAF, BAF, and BCAF. In these commensurate phases, the biquadratic interaction term effectively creates the anisotropy of the NN magnetic exchange interactions by taking a mean-field decoupling.[20] Depending on the spin alignment of two NN sites, $J_{1a}=J_1+2KS^2$ if it is AF and $J_{1b}=J_1-2KS^2$ if it is FM. Therefore, effectively, our model becomes a $J_{1a}-J_{1b}-J_2-J_3-J_c$ model in these phases. Experimentally, the spin-wave excitations in the parent compounds, $CaFe_2As_2$[11] and $BaFe_2As_2$,[16] were fitted well to the $J_{1a}-J_{1b}-J_2-J_c$ model.

The BAF and BCAF are degenerate in the classical limit. Even if we consider our model as a quantum spin model, the energy difference between two phases due to quantum fluctuations are extremely small (See Appendix D). Therefore the degeneracy between them can be broken when the couplings to other degrees of freedom are included. For FeTe, the development of the BCAF order is strongly tied to a monoclinic lattice distortion.[6,7] This monoclinic distortion breaks the same rotational symmetry of the BCAF. Therefore it lowers the energy of the BCAF state. This explains why the magnetic order transition in FeTe is a strong first-order type.[6,7] If the transition is a pure magnetic origin, the phase transition would be a weak first-order or a second-order type. In the presence of $\sqrt{5}\times\sqrt{5}$ vacancy ordering, the magnetic frustration is strongly reduced. As the vacancy ordering does not break rotational symmetry, the BAF order becomes the BAF_v phase.[35] In both FeTe and $K_{0.8}Fe_{1.6}Se_2$, the spin-wave excitations can be fitted well to a $J_{1a}-J_{1b}-J_2-J_3-J_c$ model.[10,12]

TABLE I. The values of the magnetic exchange interactions in $J_1 - J_2 - J_3 - K$ model obtained from the experimental results of different parent compounds of iron-based superconductors.[10–12,16]

Material	Phases	(Q_x, Q_y)	J_1S	J_2S	J_3S	KS^2	J_cS
$CaFe_2As_2$	CAF	$(0,1)\pi$	22	19	...	14	5
$BaFe_2As_2$	CAF	$(0,1)\pi$	25	14	...	17	2
FeTe	BCAF	$(\frac{1}{2},\frac{1}{2})\pi$	−34	18.5	9.5	9	...
$K_{0.8}Fe_{1.6}Se_2$	BAF_v	$(\frac{3}{5},\frac{1}{5})\pi$	−10	16	9	12	1.4

From the experimental results of spin-wave excitations,[10–12,16] we now can extract the magnetic exchange parameters of our model for different parent compounds. The results are summarized in Table I. We note that FeTe is near the boundary of the BCAF phase and incommensurate phases. The values listed in Table I are within the error bar of experimental values in Ref. 12. This table displays a central message that all iron-based superconductors share a similar AF NNN exchange interaction J_2. However, the sign of J_1 is different between ferropnictides and ferrochalcogenides and a significant AF J_3 exists in ferrochalcogenides but not in ferropnictides.

Second, we discuss incommensurate phases. The model also predicts three incommensurate phases. Two of them, the (π,q) and (q,q) phase have been observed. The $(0,q)$ phase is rather similar to (π,q) phase. Spin excitations in these three phases generally include two branches, which can be identified as an acoustic mode and an optical mode. Since there are neutron scattering experiments on the (π,q) phase,[34] we take it as an example. We plot their typical dispersions of two modes in Figs. 3(a) and 3(b). If we calculate the imaginary part of dynamic spin susceptibility, the quality measured by neutron scattering, an hour-glass-like behavior along this direction becomes prominent at low energy as shown in Fig. 3(c). This behavior has been recently reported in $FeSe_{0.4}Te_{0.6}$[36] and a clear explanation was not given before. The dispersion along (δ,π) as varying δ has much larger energy dispersion than the one along (π,δ) and reaches maximum at (π,π), which is consistent with experimental results observed in Ref. 31 as shown in Fig. 3(c). More detailed spin-wave properties are included in the appendixes (B, C, and D). These distinct features can be used to determine the effective magnetic exchange couplings even if the incommensurate order is not static.

IV. ELECTRONIC NEMATISM

Finally, we discuss electronic nematism induced by magnetic frustrations in the model. The CAF states break the C^4 rotational symmetry of the tetragonal lattice. The rotational symmetry breaking can be separately described by an Ising or nematic order as shown in Refs. 18 and 19. Without the specific biquadratic term K, when the parameters of the $J_1 - J_2 - J_c$ model are fixed in the CAF phase region, a weak biquadratic term can be developed through the "order by disorder" mechanism[18,19,37] by quantum fluctuations and the nematic phase transition can take place at a transition temperature T_N higher than the CAF transition temperature T_c if the interlayer coupling J_c is much weaker than J_2.[18] This physics can be analytically described in the continuum limit. As shown in Ref. 18, the effective field theory of the $J_1 - J_2 - J_c$ model in the continuum limit is given by

$$H_{\rm CAF} = \int d^2\mathbf{r} \sum_{n,\alpha} \left[\frac{1}{2} J_2 \left| \nabla \vec{\phi}_n^{\alpha}(\mathbf{r}) \right|^2 - J_c \vec{\phi}_n^{\alpha}(\mathbf{r}) \cdot \vec{\phi}_{n+1}^{\alpha}(\mathbf{r}) \right] - g \sum_n \left[\vec{\phi}_n^1(\mathbf{r}) \cdot \vec{\phi}_n^2(\mathbf{r}) \right]^2 + J_1 \sum_n \vec{\phi}_n^1(\mathbf{r}) \partial_x \partial_y \vec{\phi}_n^2(\mathbf{r}), \tag{2}$$

where we use the same notions as Ref. 18: $\vec{\phi}_n^{\alpha=1,2}$ specify the two AF Neel orders in the two sublattices of the tetragonal

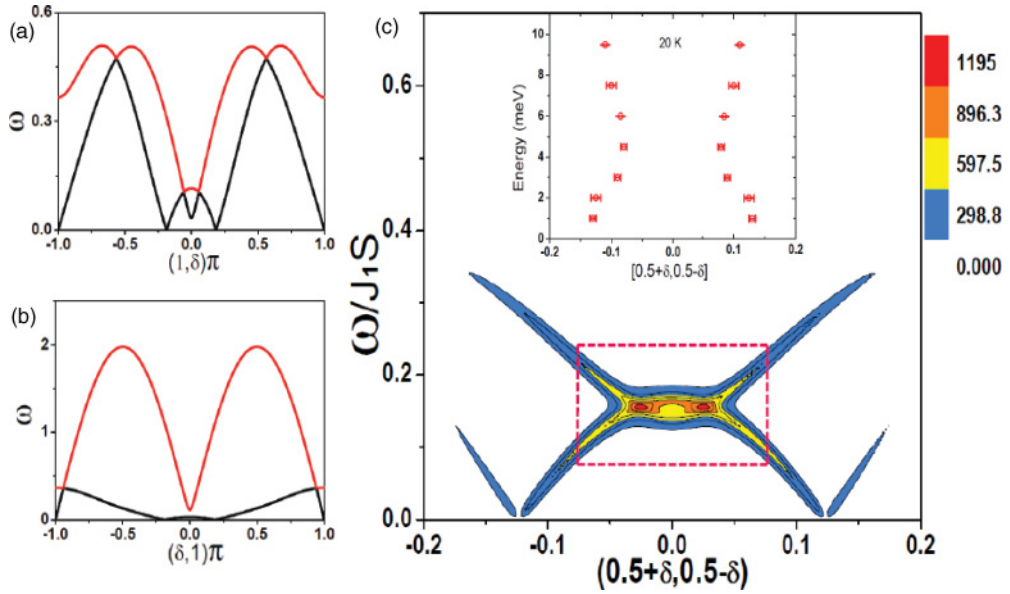

FIG. 3. (Color online) (a) and (b) Spin waves in the (π,q) incommensurate phases along $(1,\delta)\pi$ and $(\delta,1)\pi$, respectively. (c) Hour-glass-like spin waves along $(1/2+\delta,1/2-\delta)_{\rm T}$ in the (π,q) phase. The parameters are taken as $S=1, (J_1, J_2/|J_1|, J_3/|J_1|, KS^2/|J_1|) = (1, 0.6, 0.06, 0.02)$.

lattice shown in Fig. 1(a) (for simplicity, we take $S = 1$ in this section). The nematic order is defined to be $\sigma = 2g\langle\vec{\phi}_n^1(\mathbf{r}) \cdot \vec{\phi}_n^2(\mathbf{r})\rangle$. Without the biquadratic term K, $g \sim 0.13J_1^2/J_2$. With this term, we just need to modify $g \sim 0.13J_1^2/J_2 + K$. Therefore the calculations and the results in Ref. 18 are still valid. The large g value due to the specific biquadratic K term simply enhances the nematic order and increases the temperature range of spin nematic fluctuation above T_N, which has been observed experimentally.[16] In the case of BCAF or BAF states, the effective field theory model for $J_1 - J_2 - J_3$ model has also been derived in Ref. 38. With the biquadratic K term, similar to the CAF case, the effective field theory[38] essentially remains valid.

V. DISCUSSION AND CONCLUSION

By describing the magnetism of the different parent compounds of iron-based superconductors in a single effective magnetic model, we can cast insight on the microscopic origin of magnetism. First, from the magnetic exchange coupling parameters of the effective model, it is very clear that the magnetism is neither purely local nor purely itinerant, rather it is a complicated mix of the two. The presence of significant NNNN coupling J_3 suggests the local exchange mechanisms such as superexchange or double exchange are not enough to account for all magnetic exchange interactions. Moreover, the sign change of J_1 between ferropnictides and ferrochacogenides suggests that the NN exchange interactions are sensitive to subtle difference in band structures. However, the robustness of NNN J_2 interactions indicates that the NNN J_2 coupling is most likely determined by local superexchange mechanism. Second, the model reveals the significant difference between ferropnictides and ferrochacogenides: the sign difference of J_1 and the large AF J_3 in ferrochcogenides. These significant differences may suggest the importance of the p orbitals of As or Te/Se on the influence of magnetism. So far, most theoretical models are constructed based on the d orbitals of irons with onsite interactions. Since the effect of electron-electron correlations is believed to be weaker in ferropnictides than in ferrochalcogenides, one would expect the range of magnetic interactions should be shorter in ferrochalcogenides than in ferropnictides, which contradicts the existence of large J_3 interactions in ferrochalcogenides but not in ferropnictides. This contradictory can be resolved if the significant parts of magnetic exchange interactions are generated through the p orbitals of As or Se/Te. The effective magnetic exchange interactions obtained from onsite electron-electron interactions are not enough to account for entire magnetic exchange couplings. This also explains why magnetism is so sensitive to the distance of As or Se/Te away from iron planes[39] because the distance may strongly affect the mixture of p orbitals in electronic structure. Third, the model, as an effective low-energy model of magnetism, also tells us the power and limitation of LDA calculations performed for iron-based superconductors where the effect of electron-electron correlation can not be ignored. Without any doubt, the LDA calculations explain many magnetic properties in iron-based superconductors. For ferropnictides, the LDA results of J_{1a}, J_{1b}, and J_2 values are in a good agreement with experiments.[22] However, LDA calculation wrongly predicted the large anisotropy of J_2 in the BCAF and BAF states.[27,28] This failure is not surprising since the LDA in magnetically ordered state is simply a complicated mean-field approach. Finally, it has been shown that the high-energy magnetic excitations in electron-doped ferropnictides are very similar to those of parent compounds.[40] This proves that the short-range magnetic correlations in superconducting states are still dominated by the magnetic exchange interactions determined in the corresponding parent compounds. The doping destroys the long-range magnetic correlation but not the short-range interactions. Especially, the J_2 magnetic exchange interactions should be expected to vary little against doping. In $FeTe_{1-x}Se_x$, the incommensurate spin excitations are rather robust against the replacement of Te by Se.[31,32] This fact suggests that J_3 is relatively stable against the replacement in this family of materials as well. Therefore, if AF exchange couplings are responsible for superconductivity, we expect both J_2 and J_3 play a significant role in superconductivity of ferrochacolgenides.

In summary, we construct a minimum effective magnetic model that captures all the phases in iron-based superconductors. BAF magnetic states are also predicted. [Recently, the BAF state in our model has been used to explain the broken symmetry state observed in scanning tunneling microscopy (STM) results for KFe_2Se_2).[41]

ACKNOWLEDGMENTS

We are grateful to S. Kivelson, P. C. Dai, D. L. Feng, H. Ding, X. H. Chen, T. Xiang, and N. L. Wang for fruitful discussions. The research is supported by NSFC-11190024.

APPENDIX A: EXACT CLASSICAL GROUND-STATE PHASE DIAGRAM

Treating the above model classically, we can obtain the exact ground state and its phase diagram. The inplane unit cell of iron-based superconductors is determined by two basis vectors $\hat{e}_1 = (1,1)/\sqrt{2}$ and $\hat{e}_2 = (-1,1)/\sqrt{2}$. We define two relative spin-polarization angles ϕ_1 and ϕ_2 along the two basis vectors. Defining $\tilde{K} = KS^2/J_1$, $\tilde{J}_2 = J_2/J_1$, $\tilde{J}_3 = J_3/J_1$, $\lambda = \tilde{K} - 2\tilde{J}_3$, $\phi_1 = Q_x - Q_y$, and $\phi_2 = Q_x + Q_y$, we can write the classical energy of the model as

$$\tilde{e}_c = \frac{e_c}{J_1S^2} = -4\tilde{J}_3 - 2\lambda(\cos^2 Q_x + \cos^2 Q_y) + 4\tilde{J}_2\cos Q_x\cos Q_y + 2(\cos Q_x + \cos Q_y), \quad \text{(A1)}$$

which is symmetric when exchanging Q_x and Q_y. The ground-state energies of the incommensurate phases are determined by minimizing $\tilde{e}_c$. We list the solutions as follows: (i) $\tilde{e}_c = 2 - 2\tilde{K} + \frac{1}{2\lambda}(2\tilde{J}_2 + 1)^2$ for $(q,0)$ phase with $q = \arccos(\frac{2\tilde{J}_2+1}{2\lambda})$, (ii) $\tilde{e}_c = -2 - 2\tilde{K} + \frac{1}{2\lambda}(2\tilde{J}_2 - 1)^2$ for (q,π) phase with $q = \arccos(\frac{1-2\tilde{J}_2}{2\lambda})$, and (iii) $\tilde{e}_c = -4\tilde{J}_3 - \frac{1}{\tilde{J}_2-\lambda}$ for (q,q) phase with $q = \arccos[\frac{-1}{2(\tilde{J}_2-\lambda)}]$.

The energies of the commensurate phases are (i) $\tilde{e}_c = 4 - 4\tilde{K} + 4\tilde{J}_2 + 4\tilde{J}_3$ for FM phase with $(Q_x, Q_y) = (0,0)$, (ii) $\tilde{e}_c = -4\tilde{K} - 4\tilde{J}_3$ for BCAF phase with $(Q_x, Q_y) = (\pm\pi/2, \pm\pi/2)$, (iii) $\tilde{e}_c = -4\tilde{K} - 4\tilde{J}_2 + 4\tilde{J}_3$ for CAF phase

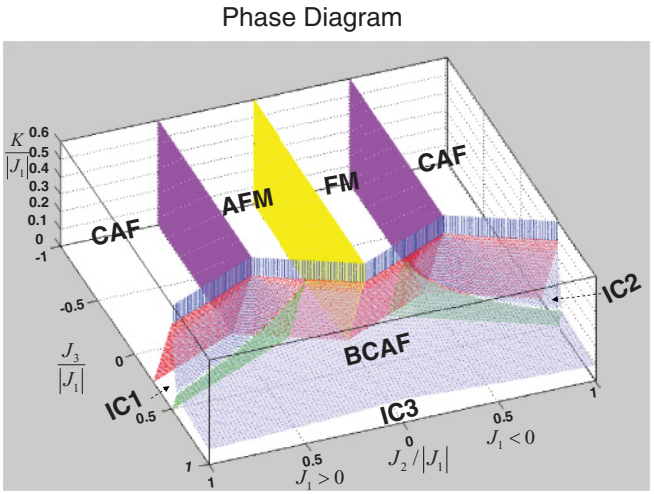

FIG. 4. (Color online) The three-dimensional $J_3/|J_1|$-$J_2/|J_1|$-$KS^2/|J_1|$ phase diagram with $S=1$. The exchange coupling J_2 is fixed to be antiferromagnetic, namely, positive.

with $(Q_x,Q_y)=(\pi,0)$, and (iv) $\tilde{e}_c=-4-4\tilde{K}+4\tilde{J}_2+4\tilde{J}_3$ for Néel (AFM) phase with $(Q_x,Q_y)=(\pi,\pi)$.

By comparing the energies of different states, we can determine the phase boundaries: (i) $\tilde{J}_2=0.5$ between AFM and CAF, (ii) $\tilde{J}_3=-\frac{1}{2}\tilde{J}_2+\frac{1}{2}\tilde{K}+\frac{1}{4}$ between AFM and (q,q), (ii) $\tilde{J}_3=-\frac{1}{2}\tilde{J}_2+\frac{1}{2}\tilde{K}+\frac{1}{8\tilde{K}}$ between BCAF and (q,q), (iv) $\tilde{J}_3=\frac{1}{4}+\frac{1}{2}\sqrt{(\tilde{K}-\frac{1}{2})^2+(\tilde{J}_2-\frac{1}{2})^2}$ between (q,π) and BCAF, (v)$\tilde{J}_3=\frac{1}{2}\tilde{J}_2+\frac{1}{2}\tilde{K}-\frac{1}{4}$ between (q,π) and CAF, (vi) $\tilde{J}_3=-\frac{1}{2}\tilde{J}_2+\frac{1}{2}\tilde{K}+\frac{1}{4}$ between (q,π) and AFM, and (vii)$\tilde{J}_3=\frac{1}{2}\tilde{J}_2+\frac{1}{2}\tilde{K}$ between (q,π) and (q,q) phases.

While the biquadratic term vanishes, the phase diagram composes of phases AFM, FM, CAF, (q,q)(IC3), (q,π)(IC1), $(q,0)$(IC2), as shown in Fig. 4. The BCAF phase appears when $\tilde{K}>1.5-\sqrt{2}$ and $\tilde{J}_3\geqslant 1/4$. The condition for observing the (q,π), $(q,0)$, and (q,q) phases is given by $\tilde{K}\leqslant\frac{1}{2}$ and they vanish from the phase diagram simultaneously at $\tilde{K}=1/2$. The phase boundaries between the commensurate phases are independent on $\tilde{K}$. Therefore the phase diagram does not change when $\tilde{K}\geqslant 1/2$.

We note that the phase diagram obtained above is the exact phase diagram of the model in the classical limit. This can be proved by a standard method for solving a classical model. For any translation invariant Hamiltonian, one can rewrite the Hamiltonian by the sum of local Hamiltonians defined in each supercell as $H=\sum_i H_i$, where i is the index of supercell. The size of the supercell depends on the range of couplings [in our case, the longest range is J_3, so it will be limited to 3×3 (total nine sites)] and the local Hamitonian has the same form with respect to the translation of the supercell. Then, one can show that the ground states we obtained are also ground states of each H_i. Thus it proves that the state is a ground state. The method is not valid for the quantum model since H_is do not communicate with each other in general.

APPENDIX B: LINEAR SPIN WAVE THEORY-LARGE S LIMIT

The inplane part of the model Hamiltonian under the linear spin-wave approximation reads

$$H=Ne_c-\frac{1}{2}\sum_k \mathrm{Tr}\mathcal{H}_k+\frac{1}{2}\sum_k \Psi_k^\dagger\mathcal{H}_k\Psi_k$$
$$=Ne_0+\sum_k\sum_{n=1}^{2}\omega_{n,k}\alpha_{n,k}^\dagger\alpha_{n,k}, \quad \text{(B1)}$$

where $e_0=e_c-\frac{1}{2N}\sum_k \mathrm{Tr}\mathcal{H}_k$ is the ground-state energy, $\Psi_k^\dagger=(b_{1,k}^\dagger,b_{2,k}^\dagger,b_{1,-k},b_{2,-k})$ and

$$\mathcal{H}_k=\begin{pmatrix} A_k & C_k & D_k & B_k \\ C_k^* & A_k & B_k^* & D_k \\ D_k & B_k & A_k & C_k \\ B_k^* & D_k & C_k^* & A_k \end{pmatrix} \quad \text{(B2)}$$

with C^* denotes the complex conjugate of C. The general form of the eigenvalues is given by

$$\omega_{1,k}=\sqrt{A^2-|B|^2+|C|^2-D^2+\sqrt{4(AC-BD)(AC^*-B^*D)-|BC^*-B^*C|^2}}, \quad \text{(B3)}$$

$$\omega_{2,k}=\sqrt{A^2-|B|^2+|C|^2-D^2-\sqrt{4(AC-BD)(AC^*-B^*D)-|BC^*-B^*C|^2}}. \quad \text{(B4)}$$

APPENDIX C: SPIN-WAVE EXCITATIONS IN INCOMMENSURATE STATES

Since the spin wave in commensurate states has been studied, we focus on the features in the spin-wave excitations of the incommensurate states. In order to compare with experimental results, it is convenient to have a table (see Table II) that lists the corresponding ordered wave vectors defined in the tetragonal unit cell and the conventional unit of square lattice.

Generally, the spin-wave excitations in incommensurate states and the corresponding Bogliubov transformation matrix are written as

$$\omega_-=\sqrt{(A^2+C^2-B^2-D^2)-2|AC-BD|}, \quad \text{(C1)}$$

$$\omega_+=\sqrt{(A^2+C^2-B^2-D^2)+2|AC-BD|}, \quad \text{(C2)}$$

and

$$\begin{pmatrix}\alpha_{1,k}\\ \alpha_{2,k}\end{pmatrix}=\begin{pmatrix}-a & a & -c, & c\\ -b & -b & d, & d\end{pmatrix}\Psi_k \quad \text{(C3)}$$

with

$$a,b = \frac{\omega_{\mp} + (A \mp C)}{2\sqrt{\omega_{\mp}(\omega_{\mp} + A \mp C)}}\text{sign}(B \mp D), \quad c,d = \frac{|B \mp D|}{2\sqrt{\omega_{\mp}(\omega_{\mp} + A \mp C)}}. \tag{C4}$$

The matrix elements can be specified as

$$\begin{aligned} A_k = &-J_1 S[\cos(Q_x) + \cos(Q_y)] + KS^2[3\cos^2(Q_x) + 3\cos^2(Q_y) - 2] \\ &+ \frac{1}{2}J_2 S\{[\cos(Q_x - Q_y) + 1]\cos(k_x - k_y) + [\cos(Q_x + Q_y) + 1]\cos(k_x + k_y) - 4\cos(Q_x)\cos(Q_y)\} \\ &+ \frac{1}{2}J_3 S\{[\cos(2Q_y) + 1]\cos(2k_y) + [\cos(2Q_x) + 1]\cos(2k_x) - 4\cos(Q_x - Q_y)\cos(Q_x + Q_y)\}, \end{aligned} \tag{C5}$$

$$\begin{aligned} B_k = &\left[-KS^3\cos(2Q_x) + \left(\frac{1}{2}J_1 S + KS^3\right)\cos(Q_x) - \frac{1}{2}J_1 S\right]\cos(k_x) \\ &+ \left[-KS^3\cos(2Q_y) + \left(\frac{1}{2}J_1 S + KS^3\right)\cos(Q_y) - \frac{1}{2}J_1 S\right]\cos(k_y), \end{aligned} \tag{C6}$$

$$\begin{aligned} C_k = &\left[-KS^3\cos(2Q_x) + \left(\frac{1}{2}J_1 S - KS^3\right)\cos(Q_x) + \frac{1}{2}J_1 S\right]\cos(k_x) \\ &+ \left[-KS^3\cos(2Q_y) + \left(\frac{1}{2}J_1 S - KS^3\right)\cos(Q_y) + \frac{1}{2}J_1 S\right]\cos(k_y), \end{aligned} \tag{C7}$$

and

$$\begin{aligned} D_k = &-KS^3[\sin^2(Q_x) + \sin^2(Q_y)] + \frac{1}{2}J_2 S\{[\cos(Q_x - Q_y) - 1]\cos(k_x - k_y) + [\cos(Q_x + Q_y) - 1]\cos(k_x + k_y)\} \\ &+ \frac{1}{2}J_3 S\{[\cos(2Q_y) - 1]\cos(2k_y) + [\cos(2Q_x) - 1]\cos(2k_x)\}. \end{aligned} \tag{C8}$$

1. (q,π) phase

Given $\tilde{K}$, the (q,π) phase region is determined by

$$\begin{aligned} &\Theta\left(\tilde{J}_2 - \frac{1}{2}\right)\left(\frac{1}{2}\tilde{K} + \frac{1}{2}\tilde{J}_2 - \frac{1}{4}\right) + \Theta\left(-\tilde{J}_2 + \frac{1}{2}\right)\left(\frac{1}{2}\tilde{K} - \frac{1}{2}\tilde{J}_2 + \frac{1}{4}\right) < \tilde{J}_3 < \Theta\left(\tilde{J}_2 - \frac{1}{8\tilde{K}}\right) \\ &\times\left[\frac{1}{4} + \frac{1}{2}\sqrt{\left(\tilde{K} - \frac{1}{2}\right)^2 + \left(\tilde{J}_2 - \frac{1}{2}\right)^2}\right] + \Theta\left(-\tilde{J}_2 + \frac{1}{8\tilde{K}}\right)\left(\frac{1}{2}\tilde{K} + \frac{1}{2}\tilde{J}_2\right), \end{aligned} \tag{C9}$$

with $\Theta(x)$ the Heaviside function. To compare with experimental results, we rewrite $(Q_x,Q_y) = (2\delta,1)\pi$ corresponding to $(a,b)_{\text{T}} = (1/2+\delta,1/2-\delta)$, which is often used in experimental plots. For the $(2\delta,1)\pi$ phase, the incommensurate angle $\delta = \frac{1}{2\pi}\arccos\frac{-\tilde{J}_2+1/2}{\tilde{K}-2\tilde{J}_3} \in [0,1/2]$. The CAF phase appears when $\delta = 0$ and Neel order occurs when $\delta = 1/2$. We only consider cases with $\delta > 0$ because the spin waves are generally symmetric about δ and $-\delta$. The incommensurate order wave vectors are close to the characteristic wave vectors of CAF when $\delta < 1/4$ and become closer to that of AFM when $\delta > 1/4$. The incommensurate magnetic excitations in $FeTe_{1-x}Se_x$ are related to the former case. In Figs. 5–7, we plot the typical magnetic excitations and their inelastic neutron scattering (INS) intensities.

2. (q,q) phase

The phase boundaries of the (q,q) phase are determined by

$$\begin{aligned} &\Theta\left(\tilde{J}_2 - \frac{1}{4}\right)\left(\frac{1}{2}\tilde{K} + \frac{1}{2}\tilde{J}_2\right) + \Theta\left(\frac{1}{4} - \tilde{J}_2\right)\left(-\frac{1}{2}\tilde{J}_2 + \frac{1}{2}\tilde{K} + \frac{1}{4}\right) < \tilde{J}_3 < -\frac{1}{2}\tilde{J}_2 + \frac{1}{2}\tilde{K} + \frac{1}{8\tilde{K}}, \quad J_1 > 0, \\ &\Theta\left(\tilde{J}_2 + \frac{1}{4}\right)\left(-\frac{1}{2}\tilde{J}_2 + \frac{1}{2}\tilde{K} - \frac{1}{4}\right) + \Theta\left(-\frac{1}{4} - \tilde{J}_2\right)\left(\frac{1}{2}\tilde{K} + \frac{1}{2}\tilde{J}_2\right) > \tilde{J}_3 > -\frac{1}{2}\tilde{J}_2 + \frac{1}{2}\tilde{K} + \frac{1}{8\tilde{K}}, \quad J_1 < 0. \end{aligned} \tag{C10}$$

The order wave vectors $(Q_x,Q_y) = (\delta,\delta)\pi$ are given by $\delta = \frac{1}{\pi}\arccos\frac{-1}{2(\tilde{J}_2-\tilde{K}+2\tilde{J}_3)}$. AFM phase occurs when $\delta = 1$ and FM phase appears when $\delta = 0$. However, the (q,q) order can not continuously transform to BCAF phase.

TABLE II. The correspondence of ordered wave vectors defined with the tetragonal unit cell and the conventional unit of square lattice.

phases	$(a,b)_{\mathrm{T}}$	(Q_x,Q_y)
BCAF	$(1/2,0)$	$(1/2,1/2)\pi$
CAF	$(1/2,1/2)$	$(0,1)\pi$
Neel	$(1,0)$	$(1,1)\pi$
(q,π)	$(1/2+\delta,1/2-\delta)$	$(2\delta,1)\pi$
$(q,0)$	$(\delta,-\delta)$	$(2\delta,0)\pi$
(q,q)	$(\delta,0)$	$(\delta,\delta)\pi$

The two spin excitation modes in this phase are degenerated when $AC-BD=0$ in Eq. (C2). One can notice that the degeneracy along $k_x+k_y=\pm\pi$ can never be lifted by changing the exchange interactions, which means the degeneracy of the acoustic and optical modes always occurs in the (q,q) phase. The spin-wave excitations and their INS intensities are displayed in Figs. 8 and 9.

3. $(q,0)$ phase

The phase boundaries of $(q,0)$ phase are defined by

$$\Theta\left(\tilde{J}_2-\frac{1}{8\tilde{K}}\right)\left(\frac{\tilde{K}}{2}+\frac{\tilde{J}_2}{2}\right)+\Theta\left(-\tilde{J}_2+\frac{1}{8\tilde{K}}\right)\times\left[-\frac{1}{4}-\frac{1}{2}\sqrt{\left(\tilde{K}+\frac{1}{2}\right)^2+\left(\tilde{J}_2+\frac{1}{2}\right)^2}\right]$$
$$<\tilde{J}_3<\Theta\left(\tilde{J}_2+\frac{1}{2}\right)\left(\frac{1}{2}\tilde{K}-\frac{1}{2}\tilde{J}_2-\frac{1}{4}\right)\times+\Theta\left(-\tilde{J}_2-\frac{1}{2}\right)\left(\frac{1}{2}\tilde{K}+\frac{1}{2}\tilde{J}_2+\frac{1}{4}\right). \quad \text{(C11)}$$

For the $(2\delta,0)\pi$ phase, the incommensurate angle $\delta=\frac{1}{2\pi}\arccos\frac{\tilde{J}_2+1/2}{\tilde{K}-2\tilde{J}_3}\in[0,1/2]$. The $(q,0)$ order transforms to FM with $\delta=0$ and to CAF with $\delta=1/2$.

Figures 10 and 11 display the spin-wave excitations and their INS scattering intensities of $(q,0)$ phase.

APPENDIX D: THE SPIN WAVES OF BAF PHASE WITH NO VACANCIES

The classical ground-state energy of BAF phase with no vacancies is degenerate with that of BCAF phase. We consider the effects of quantum fluctuations on the ground-state energy of these two phases based on the linear spin-wave approximation.

The zero-point energy per spin due to spin waves in the BCAF phase is given by

$$\epsilon_{0\mathrm{BCAF}}=\frac{1}{2}\left(e_c-\frac{1}{N}\sum_k\frac{1}{2}\mathrm{Tr}\mathcal{H}_k+\frac{1}{N}\sum_k\frac{1}{2}\sum_{n=1}^{2}\omega_{n,k}\right)=e_c'+\frac{1}{2}\left(\frac{1}{N}\sum_k\frac{1}{2}\sum_{n=1}^{2}\omega_{n,k}\right), \quad \text{(D1)}$$

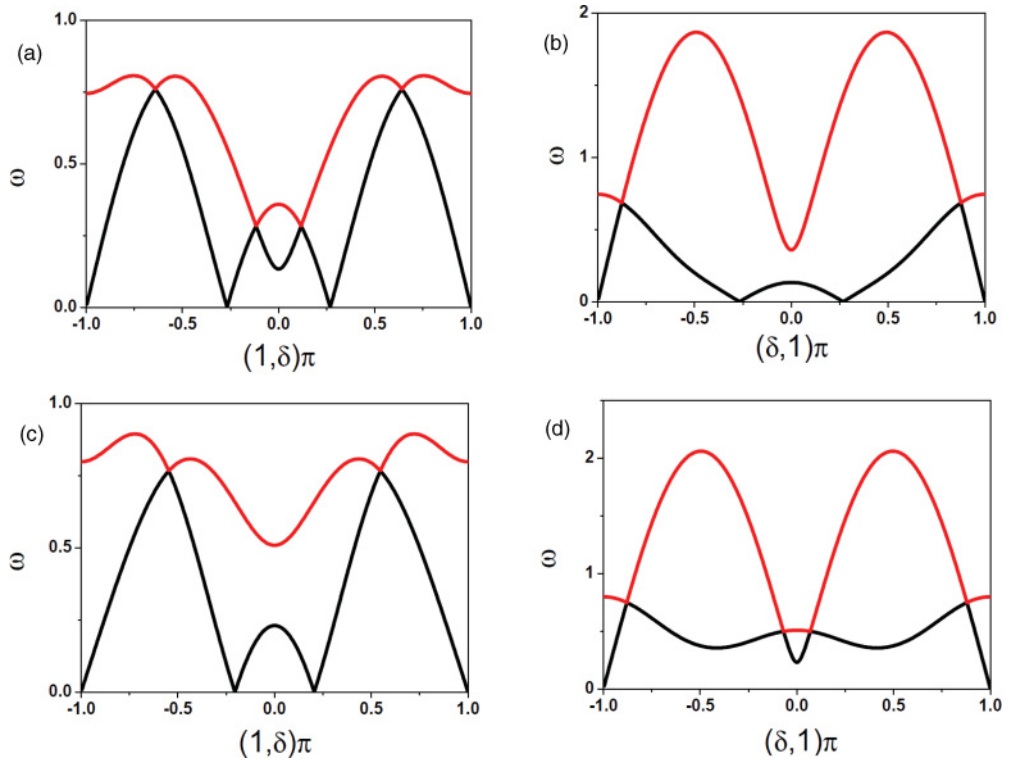

FIG. 5. (Color online) The spin-wave excitations along $(k_x,k_y)=(1,\delta)\pi$ and along $(\delta,1)\pi$ in the (π,q) phase near CAF phase. The parameters are chosen to be $S=1$ and $(J_1,\tilde{J}_2,\tilde{J}_3,\tilde{K})=(1,0.7,0.15,0)$ in (a) and (b), and $(1,0.7,0.15,0.05)$ in (c) and (d). Increasing $\tilde{K}$ (biquadratic interactions) opens a gap between the acoustic and optical modes near $(\pi,0)$ in the $(1,\delta)\pi$ direction.

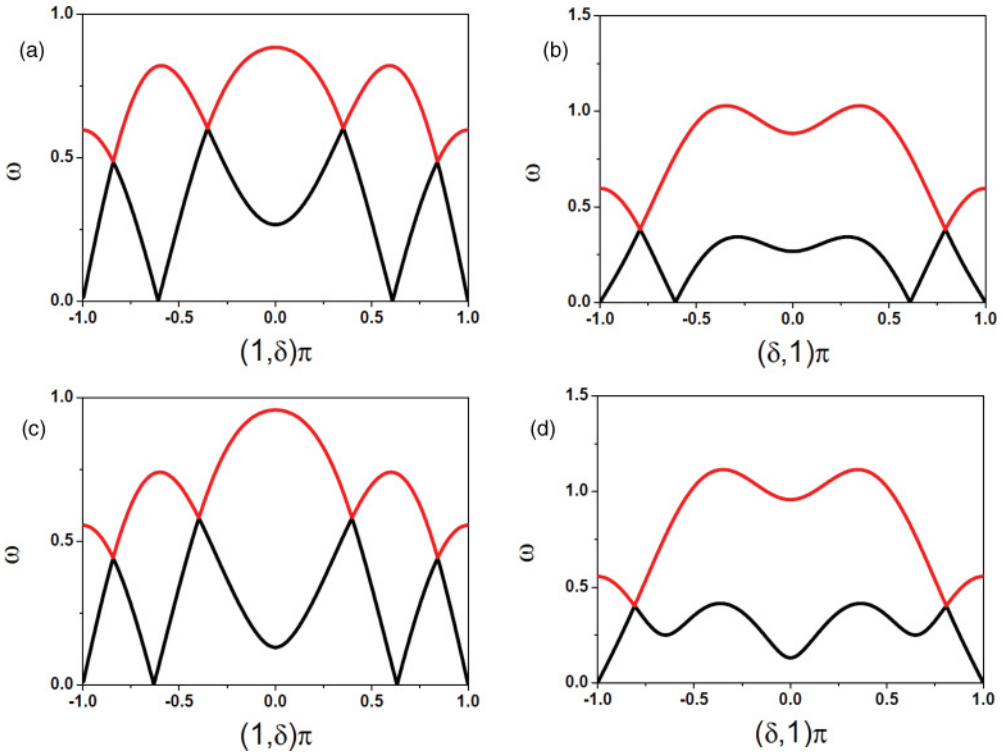

FIG. 6. (Color online) The spin-wave excitations along $(k_x,k_y)=(1,\delta)\pi$ and along $(\delta,1)\pi$ in the (π,q) phase near AFM phase. The parameters are chosen to be $S=1$ and $(J_1,\tilde{J}_2,\tilde{J}_3,\tilde{K})=(1,0.4,0.15,0)$ in (a) and (b), and $(1,0.4,0.15,0.05)$ in (c) and (d). Increasing $\tilde{K}$ has a smaller effect in the $(1,\delta)\pi$ direction but opens a gap near $(\pi/2,\pi)$ in the $(\delta,1)\pi$ direction.

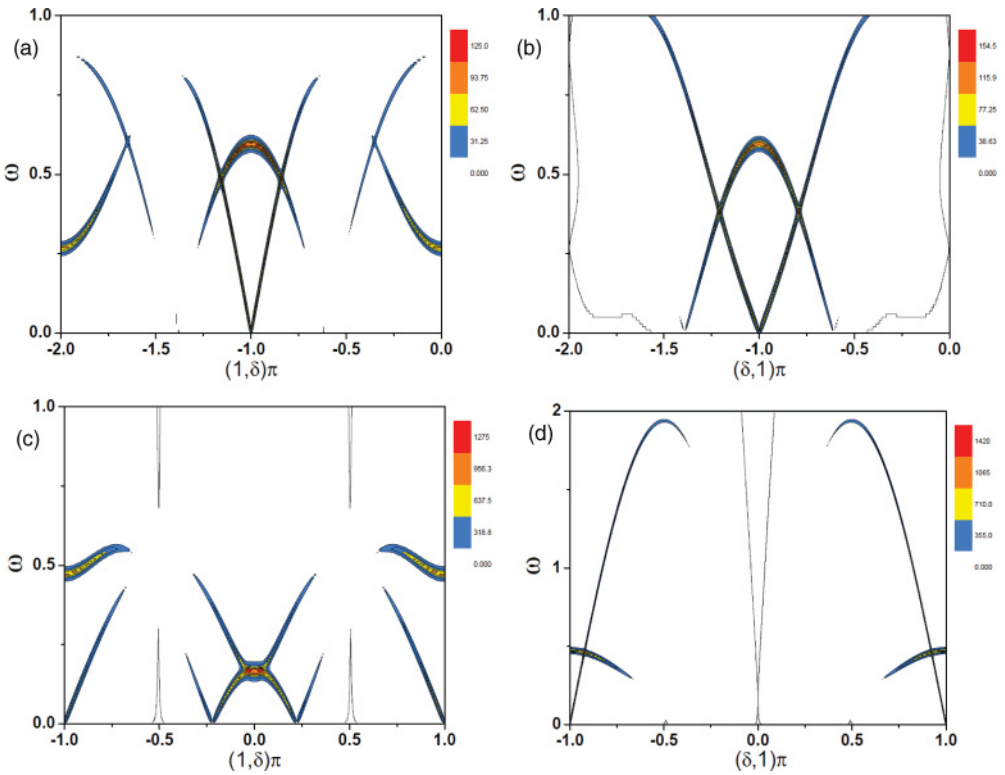

FIG. 7. (Color online) The INS intensity along $(k_x,k_y)=(1,\delta)\pi$ and along $(\delta,1)\pi$ in the (π,q) phase. (a) and (b) are close to AFM phase with parameters chosen to be $(J_1,\tilde{J}_2,\tilde{J}_3,\tilde{K})=(1,0.4,0.15,0)$, (c) and (d) are near CAF with parameters equal to $(1,0.6,0.07,0.01)$. The thin lines label the boundaries of zone with vanishing intensities.

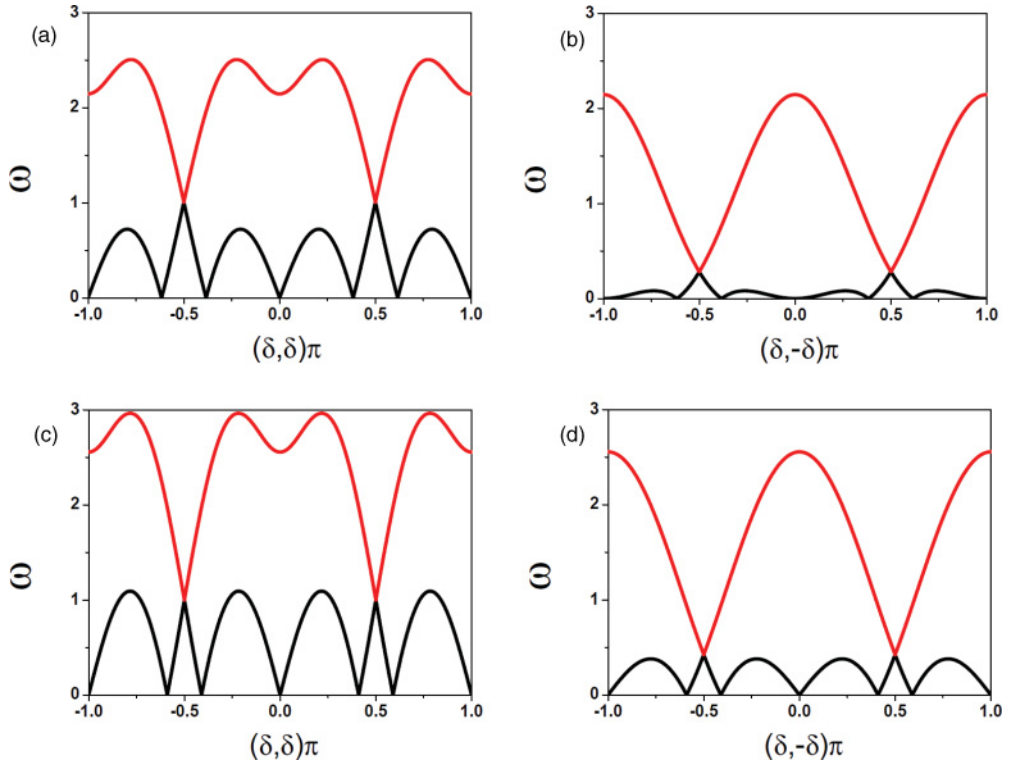

FIG. 8. (Color online) The spin-wave excitations along $(k_x,k_y) = (\delta,\delta)\pi$ and along $(\delta, -\delta)\pi$ in the (q,q) phase. The parameters are chosen to be $S = 1$ and $(J_1,\tilde{J}_2,\tilde{J}_3,\tilde{K}) = (-1,0.7,0.4,0.1)$ in (a),(b), and $(-1,0.8,0.5,0)$ in (c),(d).

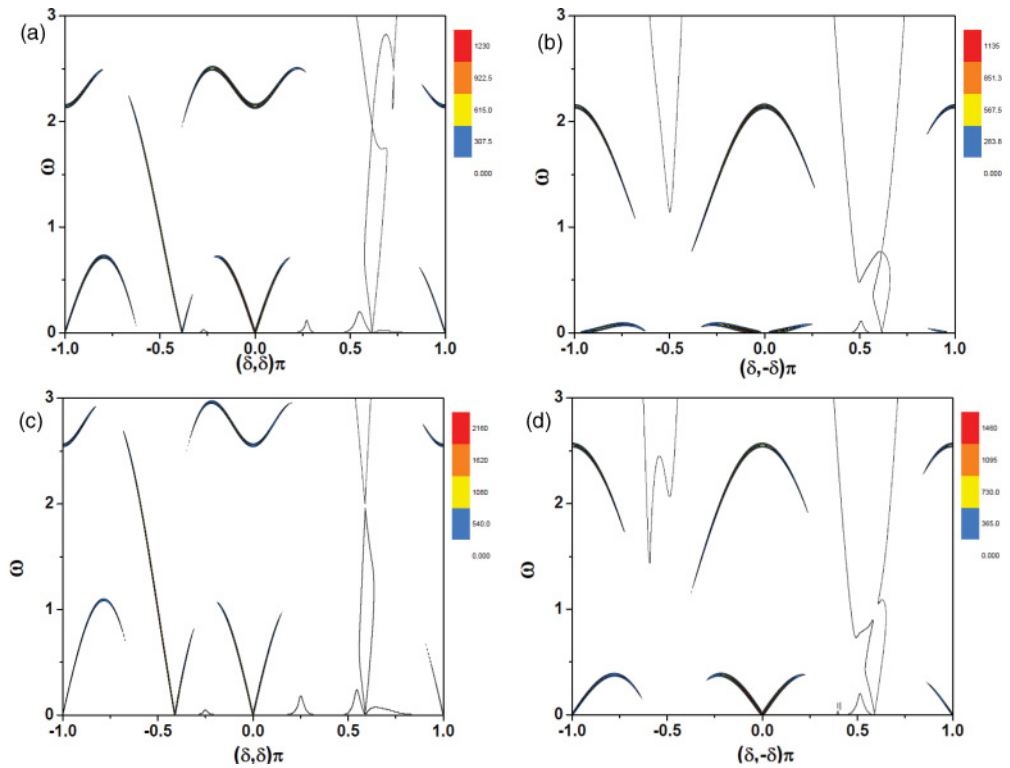

FIG. 9. (Color online) The INS intensity along $(k_x,k_y) = (\delta,\delta)\pi$ and along $(\delta, -\delta)\pi$ in the (q,q) phase. The parameters are chosen to be $S = 1$ and $(J_1,\tilde{J}_2,\tilde{J}_3,\tilde{K}) = (-1,0.7,0.4,0.1)$ in (a) and (b), and $(-1,0.8,0.5,0)$ in (c) and (d). The thin lines label the boundaries of zone with vanishing intensities.

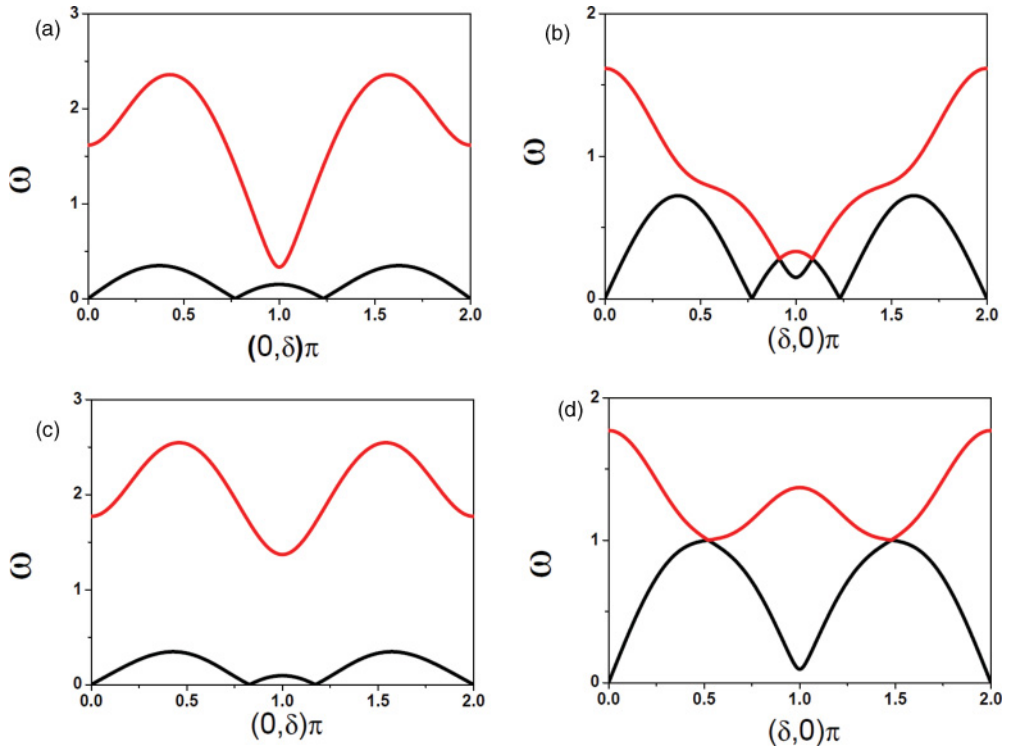

FIG. 10. (Color online) The spin-wave excitations along $(k_x,k_y) = (0,\delta)\pi$ and along $(\delta,0)\pi$ in the $(0,q)$ phase. The parameters are chosen to be $S = 1$ and $(J_1,\tilde{J}_2,\tilde{J}_3,\tilde{K}) = (-1,0.8,0.2,0.)$ in (a) and (b), and $(-1,0.8,0.2,0.05)$ in (c) and (d).

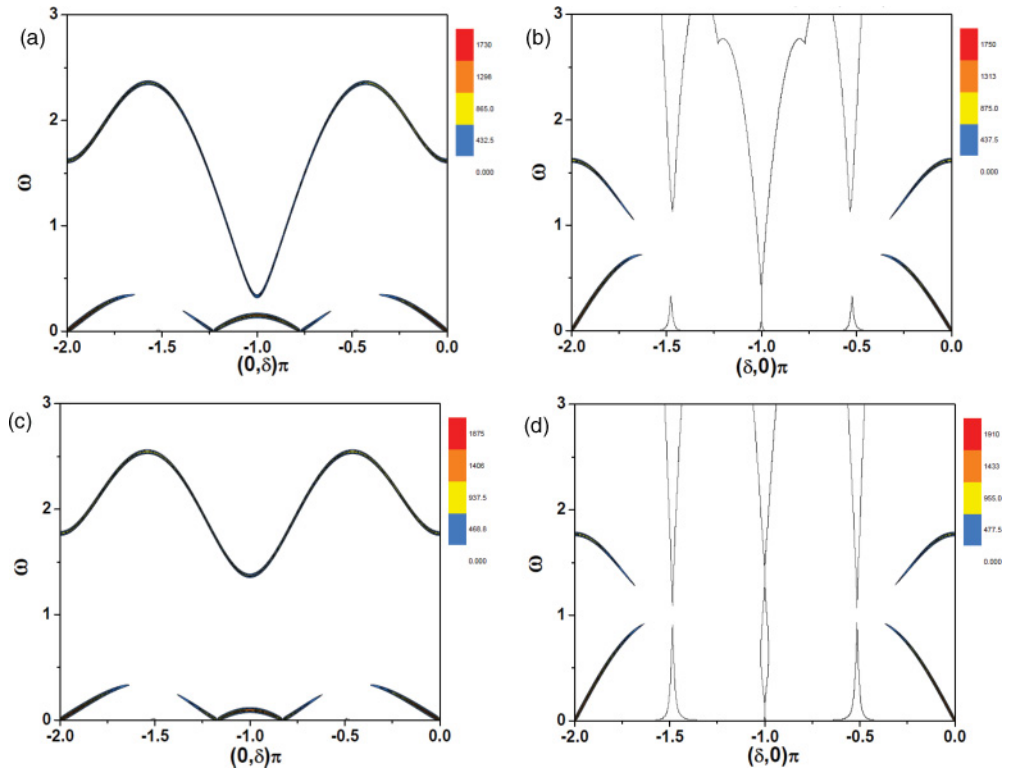

FIG. 11. (Color online) The scattering intensity along $(k_x,k_y) = (0,\delta)\pi$ and along $(\delta,0)\pi$ in the $(0,q)$ phase. The parameters are chosen to be $S = 1$ and $(J_1,\tilde{J}_2,\tilde{J}_3,\tilde{K}) = (-1,0.8,0.2,0.)$ in (a) and (b), and $(-1,0.8,0.2,0.05)$ in (c) and (d). The thin lines label the boundaries of zone with vanishing intensities.

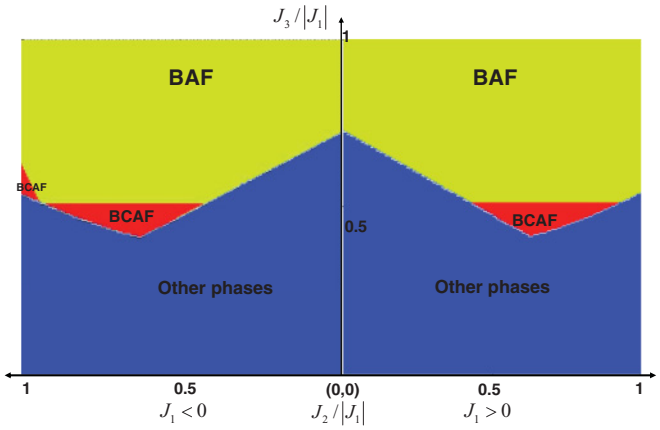

FIG. 12. (Color online) The phase diagram of the quantum model that breaks the degeneracy of the BCAF and BAF phases for $S=1$, $\tilde{K}=0.2$.

where $e_c' = -J_3S(S+2) - KS^3(S+4)$ and $\omega_{n,k}$ is determined by Eq. (B4) with $A_k = 8KS^3 + 4J_3S + \mathcal{J}_{2,k}^+$, $B_k = -\mathcal{J}_1^+(e^{-ik_x}+e^{ik_y}), C_k = \mathcal{J}_1^-(e^{ik_x}+e^{-ik_y})$, $D_k = -\mathcal{J}_{2,k}^- + \mathcal{J}_{3,k}, \mathcal{J}_1^\pm = J_1S \pm 2KS^3$, $\mathcal{J}_{2,k}^\pm = 2J_2S\cos(k_x \pm k_y)$, and $\mathcal{J}_{3,k} = -2J_3S[\cos(2k_x)+\cos(2k_y)]$.

The spin waves in the BAF state are given by

$$H = Ne_c - \frac{1}{2N}\sum_k \mathrm{Tr}\mathcal{H}_k + \frac{1}{2}\sum_k \Psi_k^\dagger \mathcal{H}_k \Psi_k$$
$$= Ne_0 + \sum_k \sum_n \tilde{\omega}_{n,k}\alpha_{n,k}^\dagger \alpha_{n,k}, \tag{D2}$$

where $\Psi_k^\dagger = (b_{1,k}^\dagger, b_{2,k}^\dagger, b_{3,k}^\dagger, b_{4,k}^\dagger, b_{1,-k}, b_{2,-k}, b_{3,-k}, b_{4,-k})$ and

$$\mathcal{H}_k = \begin{pmatrix} \lambda & \mathcal{J}_1^- e^{-ik_x} & \mathcal{J}_{2,k}^- & \mathcal{J}_1^- e^{ik_y} & \mathcal{J}_{3,k} & -\mathcal{J}_1^+ e^{ik_x} & -\mathcal{J}_{2,k}^+ & -\mathcal{J}_1^+ e^{-ik_y} \\ & \lambda & \mathcal{J}_1^- e^{ik_y} & \mathcal{J}_{2,k}^+ & -\mathcal{J}_1^+ e^{-ik_x} & \mathcal{J}_{3,k} & -\mathcal{J}_1^+ e^{-ik_y} & -\mathcal{J}_{2,k}^- \\ & & \lambda & \mathcal{J}_1^- e^{ik_x} & -\mathcal{J}_{2,k}^+ & -\mathcal{J}_1^+ e^{ik_y} & \mathcal{J}_{3,k} & -\mathcal{J}_1^+ e^{-ik_x} \\ & & & \lambda & -\mathcal{J}_1^+ e^{ik_y} & -\mathcal{J}_{2,k}^- & -\mathcal{J}_1^+ e^{ik_x} & \mathcal{J}_{3,k} \\ & & & & \lambda & \mathcal{J}_1^- e^{-ik_x} & \mathcal{J}_{2,k}^- & \mathcal{J}_1^- e^{ik_y} \\ & & & & & \lambda & \mathcal{J}_1^- e^{ik_y} & \mathcal{J}_{2,k}^+ \\ & & & & & & \lambda & \mathcal{J}_1^- e^{ik_x} \\ & & & & & & & \lambda \end{pmatrix} \tag{D3}$$

with $\lambda = 4J_3S + 8KS^3$.

Only the upper right part of the matrix is shown since the Hamiltonian is Hermitian. The zero-point energy per spin due to spin waves is given by

$$\epsilon_{0\mathrm{BAF}} = \frac{1}{4}\left(e_c - \frac{1}{N}\sum_k \frac{1}{2}\mathrm{Tr}\mathcal{H}_k + \frac{1}{N}\sum_k \frac{1}{2}\sum_{n=1}^4 \tilde{\omega}_{n,k}\right) = e_c' + \frac{1}{4}\left(\frac{1}{N}\sum_k \frac{1}{2}\sum_{n=1}^4 \tilde{\omega}_{n,k}\right). \tag{D4}$$

The difference between the zero-point energy of BAF phase and that of BCAF phase is given by

$$\delta\epsilon_0 = \frac{1}{4}\left(\frac{1}{N}\sum_k \frac{1}{2}\sum_{n=1}^4 \tilde{\omega}_{n,k}\right) - \frac{1}{2}\left(\frac{1}{N}\sum_k \frac{1}{2}\sum_{n=1}^2 \omega_{n,k}\right). \tag{D5}$$

The analytic form of the energy difference is hard to obtain. Numerically, the energy difference is in the order of $10^{-3}J_1$, a tiny value. In the large region, the BAF state has lower energy than the BCAF state. In the region close to incommensurate phases, the energy of BCAF can be lower than that of the BAF. In Fig. 12, we report numerical results for the quantum ground states of the model by taking $S=1$, $\tilde{K}=0.2$.

*jphu@iphy.ac.cn/hu4@purdue.edu

[1] Y. Kamihara, T. Watanabe, M. Hirano, and H. Hosono, J. Am. Chem. Soc. **130**, 3296 (2008).
[2] X. H. Chen, T. Wu, G. Wu, R. H. Liu, H. Chen, and D. F. Fang, Nature (London) **453**, 761 (2008).
[3] Hsu Fong-Chi, Jiu-Yong Luo, Kuo-Wei Yeh, Ta-Kun Chen, Tzu-Wen Huang, Phillip M. Wu, Yong-Chi Lee, Yi-Lin Huang, Yan-Yi Chu, Der-Chung Yan, Maw-Kuen Wu, Proc. Natl. Acad. Sci. USA **105**, 14262 (2008).
[4] Jiangang Guo, Shifeng Jin, Gang Wang, Shunchong Wang, Kaixing Zhu, Tingting Zhou, Meng He, Xiaolong Chen, Phys. Rev. B **82**, 180520 (2010).
[5] Clarina de la Cruz, Q. Huang, J. W. Lynn, Jiying Li, W. Ratcliff II, J. L. Zarestky, H. A. Mook, G. F. Chen, J. L.

Luo, N. L. Wang, and Pengcheng Dai, Nature (London) **453**, 899 (2008).
[6]W. Bao, Y. Qiu, Q. Huang, M. A. Green, P. Zajdel, M. R. Fitzsimmons, M. Zhernenkov, S. Chang, M. Fang, B. Qian, E. K. Vehstedt, J. Yang, H. M. Pham, L. Spinu, and Z. Q. Mao, Phys. Rev. Lett. **102**, 247001 (2009).
[7]Shiliang Li, Chenglin Zhang, Meng Wang, Hui-qian Luo, Xingye Lu, Enrico Faulhaber, Astrid Schneidewind, Peter Link, Jiangping Hu, Tao Xiang, and Pengcheng Dai, Phys. Rev. Lett. **105**, 157002 (2010).
[8]Wei Bao, Q. Huang, G. F. Chen, M. A. Green, D. M. Wang, J. B. He, X. Q. Wang, and Y. Qiu, Chin. Phys. Lett. **28**, 086104 (2011).
[9]J. J. Ying, X. F. Wang, X. G. Luo, A. F. Wang, M. Zhang, Y. J. Yan, Z. J. Xiang, R. H. Liu, P. Cheng, G. J. Ye, and X. H. Chen, Phys. Rev. B **83**, 212502 (2011).
[10]Miaoyin Wang, Chen Fang, Dao-Xin Yao, GuoTai Tan, Leland W. Harriger, Yu Song, Tucker Netherton, Chenglin Zhang, Meng Wang, Matthew B. Stone, Wei Tian, Jiangping Hu, and Pengcheng Dai, Nat. Commun. **2**, 580 (2011).
[11]Jun Zhao, D. T. Adroja, Dao-Xin Yao, R. Bewley, Shiliang Li, X. F. Wang, G. Wu, X. H. Chen, Jiangping Hu, Pengcheng Dai, Nat. Phys. **5**, 555 (2009).
[12]O. J. Lipscombe, G. F. Chen, Chen Fang, T. G. Perring, D. L. Abernathy, A. D. Christianson, Takeshi Egami, Nanlin Wang, Jiangping Hu, and Pengcheng Dai, Phys. Rev. Lett. **106**, 057004 (2011).
[13]S. O. Diallo, V. P. Antropov, T. G. Perring, C. Broholm, J. J. Pulikkotil, N. Ni, S. L. Bud'ko, P. C. Canfield, A. Kreyssig, A. I. Goldman, and R. J. McQueeney, Phys. Rev. Lett. **102**, 187206 (2009).
[14]K. Matan, R. Morinaga, K. Iida, and T. Sato, J. Phys. Rev. B **79**, 054526 (2009).
[15]L.X. Yang, Y. Zhang, H.W. Ou, J.F. Zhao, D.W. Shen, B. Zhou, J. Wei, F. Chen, M. Xu, C. He, Y. Chen, Z.D. Wang, X.F. Wang, T. Wu, G. Wu, X.H. Chen, M. Arita, K. Shimada, M. Taniguchi, Z.Y. Lu, T. Xiang, and D.L. Feng, Phys. Rev. Lett. **102**, 107002 (2009).
[16]Leland W. Harriger, Huiqian Luo, Mengshu Liu, C. Frost, Jiangping Hu, M. R. Norman, and Pengcheng Dai, Phys. Rev. B **84**, 054544 (2011).
[17]Si. Q., and E. Abrahams, Phys. Rev. Lett. **101**, 076401 (2008).
[18]C. Fang, H. Yao, W. F. Tsai, J. P. Hu, and S. A. Kivelson, Phys. Rev. B **77**, 224509 (2008).
[19]F. J. Ma, Z. Y. Lu, and T. XiangPhys. Rev. B **78**, 224517 (2008).
[20]A. L. Wysocki, K. D. Belashchenko, and V. P. Antropov, Nat. Phys. **7**, 485 (2011).
[21]I. I. Mazin and M. D. Johannes, Nat. Phys. **5**, 14115 (2009).
[22]M. J. Han, Q. Yin, W. E. Pickett, and S. Y. Savrasov, Phys. Rev. Lett. **102**, 107003 (2009).
[23]J. Dong *et al*., Europhys. Lett. **83**, 27006 (2008).
[24]W. C. Lv, F. Kroger, and P. Phillips, Phys. Rev. B **82**, 045125 (2010).
[25]C.-C. Lee, W.-G. Yin, and W. Ku, Phys. Rev. Lett. **103**, 267001 (2009).
[26]A. M. Turner, F. Wang, and A. Vishwanath, Phys. Rev. B **80**, 224504 (2009).
[27]M. J. Han and S. Y. Savrasov, Phys. Rev. Lett. **103**, 067001 (2009).
[28]C. Cao and J. Dai, e-print arXiv:1102.1344.
[29]Fengjie Ma, Wei Ji, Jiangping Hu, Zhong-Yi LU, and Tao Xiang, Phys. Rev. Lett. **102**, 177003 (2009).
[30]C. Fang, A. B. Bernevig, and J Hu, Europhys. Lett. **86**, 67005 (2009).
[31]M. D. Lumsden, A. D. Christianson, E. A. Goremychkin, S. E. Nagler, H. A. Mook, M. B. Stone, D. L. Abernathy, T. Guidi, G. J. MacDougall, C. de la Cruz, A. S. Sefat, M. A. McGuire, B. C. Sales, and D. Mandrus, Nat. Phys. **6**, 182 (2010).
[32]D.N. Argyriou, A. Hiess, A. Akbari, I. Eremin, M.M. Korshunov, J. Hu, B. Qian, Z. Mao, Y. Qiu, C. Broholm, and W. Bao, Phys. Rev. B **81**, 220503(R) (2010).
[33]D. K. Pratt, M. G. Kim, A. Kreyssig, Y. B. Lee, G. S. Tucker, A. Thaler, W. Tian, J. L. Zarestky, S. L. Bud'ko, P. C. Canfield, B. N. Harmon, A. I. Goldman, and R. J. McQueeney, Phys. Rev. Lett. **106**, 257001 (2011).
[34]C.H. Lee, K. Kihou, H. Kawano-Furukawa, T. Saito, A. Iyo, H. Eisaki, H. Fukazawa, Y. Kohori, K. Suzuki, H. Usui, K. Kuroki, and K. Yamada, Phys. Rev. Lett. **106**, 067003 (2011).
[35]C. Fang *et al*. e-print arXiv:1103.4599v2.
[36]Shiliang Li, Chenglin Zhang, Meng Wang, Hui-qian Luo, Xingye Lu, Enrico Faulhaber, Astrid Schneidewind, Peter Link, Jiangping Hu, Tao Xiang, and Pengcheng Dai, Phys. Rev. Lett. **105**, 157002 (2010).
[37]P. Chandra, P. Coleman, and A. J. Larkin, Phys. Rev. Lett. **64**, 88 (1990).
[38]Xu Cenke and Hu JP, e-print arXiv:0903.4477.
[39]Kazuhiko Kuroki, Seiichiro Onari, Ryotaro Arita, Hidetomo Usui, Yukio Tanaka, Hiroshi Kontani, Hideo Aoki, Phys. Rev. B **79**, 224511 (2009).
[40]P. C. Dai (private communication).
[41]Peng Cai, Cun Ye, Wei Ruan, Xiaodong Zhou, Aifeng Wang, Meng Zhang, Xianhui Chen, Yayu Wang, e-print arXiv:1108.2798.